Binding of the Highly Toxic Tetracycline Derivative, Anhydrotetracycline, to Bovine Serum Albumin

Martha Ines Burgos,*[,a] Ricardo Ariel Fernández,[b,#] María Soledad Celej,[a] Laura Isabel Rossi,[c] Gerardo Daniel Fidelio,[a] and Sergio Alberto Dassie[b]

[a] *Departamento de Química Biológica-Centro de Investigaciones en Química Biológica de Córdoba (CIQUIBIC), Facultad de Ciencias Químicas, Universidad Nacional de Córdoba, Ciudad Universitaria;* [b] *Departamento de Fisicoquímica-Instituto de Investigaciones en Fisicoquímica de Córdoba (INFIQC), Facultad de Ciencias Químicas, Universidad Nacional de Córdoba, Ciudad Universitaria; and* [c] *Departamento de Química Orgánica-Instituto de Investigaciones en Fisicoquímica de Córdoba (INFIQC), Facultad de Ciencias Químicas, Universidad Nacional de Córdoba, Ciudad Universitaria; X5000HUA Córdoba, Argentina.*

Received March 24, 2011; accepted April 29, 2011; published online May 23, 2011

Tetracycline (TC) derivatives are extensively used as antibiotics in human and animal medicine and, very recently, they have been screened as anti-amyloidogenic drugs. Anhydrotetracycline (AHTC) is one of the major degradation products of TC that has been linked to several side effects of the drug. We evaluated the interaction of AHTC with bovine serum albumin (BSA), one of the main carriers of amphiphilic molecules in blood, using three complementary analytical methods: fluorescence spectroscopy, isothermal titration calorimetry and differential scanning calorimetry. AHTC bound to BSA with an association constant in the order of 10^5 M^{-1}. Drug binding was enthalpically and entropically driven and seemed to involve hydrophobic interactions. AHTC fluorescence enhancement and hypsochromic shifts observed upon binding suggested a low-polarity location excluded from water for the bound drug. Our data are useful for evaluating the biodisponibility of the pharmacophore and the dynamic distribution of the toxic derivative.

Key words protein stability; ligand binding; bovine serum albumin; tetracycline; differential scanning calorimetry; isothermal titration calorimetry

Tetracycline (TC) derivatives comprise a group of bacteriostatic antibiotics extensively used in human and veterinary medicine and in acquaculture, and as animal growth promoters due to their safe toxicological profile.[1)] More recently, they have been proposed as anti-amyloidogenic drugs since they can interfere with protein conformational changes and self-assemblies associated with protein misfolding and deposition diseases.[2—4)]

Despite their popular use, TC derivatives are highly unstable and some degradation products formed during the storage or normal use of the drugs are pharmacologically toxic or inactive compounds.[5)] Anhydrotetracycline (AHTC) is one of the major degradation products of TC that has been linked to several side effects of the drug, *e.g.*, cutaneous phototoxicity[6)] and Fanconi-type syndrome.[7)] AHTC has also proven to be more toxic than TC against environmentally relevant bacteria.[8)]

AHTC can be produced by dehydration in acid media,[5,8)] by photolysis in mild reducing conditions[6,9,10)] or during high-temperature treatments.[11)] Removal of a water molecule from the C5a–C6 positions of TC by treatment with warm mineral acid gives the anhydroderivative (Fig. 1).[12)] Dehydration leads to significant changes in aromatization and planarity of the tetracyclic moiety,[13,14)] showing variations in potency,[15)] mechanism of action[1)] and lipophilicity[16,17)] as compared to the parent compound. Changes in chemical configuration can also modulate the interaction of drugs with serum proteins.[18)]

Serum albumins are the main carriers of physiological metabolites and pharmacological drugs in blood. Protein binding has a significant impact on the pharmacokinetics and biological activity of drugs and modulates the toxicity of bound substances, attenuates adverse reactions and prolongs the *in vivo* half-life of therapeutic agents.[18—21)]

The facts outlined above prompted us to investigate the interaction of AHTC with bovine serum albumin (BSA) using three biophysical techniques. Binding affinity and number of interacting ligands were assessed by fluorimetric titration.

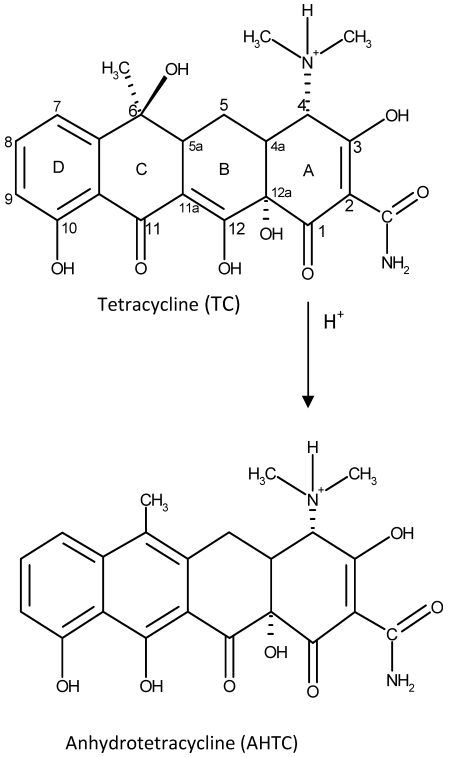


Fig. 1. Chemical Structures of Tetracycline (TC) and Anhydrotetracycline (AHTC) Indicating the Degradation Pathway of TC in Acid Solution

* To whom correspondence should be addressed. e-mail: inesburgos@fcq.unc.edu.ar
# Equal contribution with first author.

© 2011 Pharmaceutical Society of Japan

Additional isothermal titration calorimetry (ITC) measurements were performed in order to get relevant thermodynamic binding parameters, confirmed by complementary differential scanning calorimetry (DSC) experiments. The results are discussed in terms of the available data for other TC derivatives interacting with proteins.

MATERIALS AND METHODS

Chemicals Fatty acid and globulin-free BSA and tetracycline were purchased from Sigma Chemical Co. and used without further purification. AHTC was synthesised using the following procedure[12]: a solution of 2-propanol (20.2 ml), methanol (1.5 ml) and concentrated hydrochloric acid (7.2 ml) was added to tetracycline hydrochloric (2.3975 g). After refluxing for 20 min, the resulting yellow precipitate was filtered, washed with 2-propanol (3×10 ml) and dried under vacuum for 2.5 h. The crude product was then refluxed in benzene (250 ml). The remaining precipitate was filtered and dried under vacuum to yield 2.0457 g of product. The product was identified by infrared spectroscopy using a KBr disk, giving the following characteristic wavelenth signals (cm^{-1}): 3409, 3318, 3181, 3096, 3065, 1646, 1614, 1568, 1461, 1440, 1400, 1369, 1340, 1243, 1137, 1076, 618.

BSA and AHTC were dissolved in 100 mM phosphate buffer pH 7.4 prepared in ultra pure water. The concentrations were determined by UV absorption from diluted solutions using the extinction coefficients $\varepsilon_{280}=35910\ M^{-1}\,cm^{-1}$ and $\varepsilon_{430}=8900\ m^{-1}\,cm^{-1}$ for BSA and AHTC, respectively.

Fluorescence Spectroscopy Steady-state emission spectra were recorded in a SLM-Aminco 4800C spectrofluorometer equipped with a Xenon arc lamp and a thermostated cell holder. The temperature was controlled by a circulating bath and measured with a thermocouple placed into the cell. Spectra were acquired at 25 °C. Slit widths were set at 8 nm and a horizontal polarizer was placed in the emission channel. AHTC was selectively excited at 430 nm.

In titration experiments, increasing volumes of 1.7 mM AHTC were added to a solution containing 2.5 μM BSA or to buffer alone (blank) under continuous stirring. The spectra were recorded after equilibration for 3 min. Data were corrected for inner filter effects.

Titration curves were analyzed assuming a single type of binding site according to:

$$F = f_L L_{tot} + \frac{1}{2}(f_{PL_n} - f_L)(L_{tot} + nP_{tot} + K_d^{app} - \sqrt{(L_{tot} + nP_{tot} + K_d^{app})^2 - 4L_{tot}nP_{tot}}) \quad (1)$$

Where F is the fluorescence signal corrected for inner filter effects, f_L and f_{PL_n} are the apparent specific fluorescence signals for the free ligand L and the complex PL_n, L_{tot} and P_{tot} are the total ligand and protein concentrations after corrections for dilution, n is the number of binding sites and K_d^{app} is the apparent dissociation constant. To minimize the number of adjustable parameters f_L was obtained from the blank curves and held constant to fit the protein titration curves.

ITC Measurements ITC measurements were done using a VP-ITC calorimeter from MicroCal, Llc. BSA and AHTC concentrations were 20 μM and 0.7 mM, respectively. The reference cell was filled with ultra pure water. The titration of BSA with AHTC involved 37 injections of ligand solution (20×4 μl, and 17×10 μl) at 5 min intervals. The stirring rate was 300 rpm.

The heat of ligand dilution in buffer was subtracted from the titration data of BSA. Data were analyzed according to a model for a single set of binding sites included in the Origin 5.0 software provided by the manufacturer. The first injection was not taken into account for the analysis. Three independent experiments were analyzed separately and the fit parameters were averaged.

DSC Measurements Thermograms were obtained using a MicroCal VP-DSC calorimeter from MicroCal Llc. BSA concentration was 9 μM. The reference cell was filled with buffer and a 26 p.s.i. pressure was applied to both cells. A scan rate of 60 °C/h was used for all the experiments.

The calorimetric data were analyzed using the Origin 7.5 software supplied by the manufacturer. A reversible non-two-state denaturation model was used to obtain the midpoint of the thermal unfolding (T_m), the actual heat absorption during protein unfolding (ΔH_m) and the van't Hoff (ΔH_{vH}) enthalpy or effective enthalpy, which represents the theoretical heat of the transition assuming a two-state model:

$$\Delta H_{vH} = RT^2 \frac{d \ln\left(\frac{f_u}{1-f_u}\right)}{dT}$$

The cooperative unit was calculated as the ratio $\Delta H_m/\Delta H_{vH}$.[22] If the assumption that denaturation is a transition between only two states is a valid one, *i.e.* without intermediates significantly populated, the effective enthalpy should be equal to the real one and the ratio between them should be close to unity.

The applicability of equilibrium thermodynamic analysis to irreversible DSC transitions has been discussed previously.[23] Reversible unfolding models were employed to fit the data after checking that the calorimetric signal was reduced by about 40% after heating a BSA solution up to the T_m, then cooled it to room temperature and then reheated it to $T \gg T_m$ and that similar thermograms and results were obtained either (i) at different protein concentrations (ref. 24 and this work) and (ii) by fitting the entire DSC curve using only the first half of the experimental data from the endotherm.

DSC has proven to be very useful for characterizing the energetics of protein unfolding and biomolecular interactions.[25—27] We have employed the formalism described in ref. 28 to estimate the apparent binding constant (K_d^{app}) of AHTC to BSA from DSC curves acquired at different ligand/protein molar ratios. Briefly, the model assumes a two-state protein unfolding transition coupled to ligand binding to n independent sites in the native state. For every temperature, the enthalpies and constants for the unfolding and binding reactions were evaluated. Mass balance equations were solved by iterative techniques. Once the relative population of the unfolded state and the overall ligand-linked enthalpy change were computed, the average excess heat capacity change was evaluated by numerical differentiation. This sequence was coupled to a multidimensional optimization routine in order to get K_b^{app} (see ref. 28 and references therein for details). The intrinsic unfolding parameters were obtained from an endotherm of free BSA. The binding enthalpy

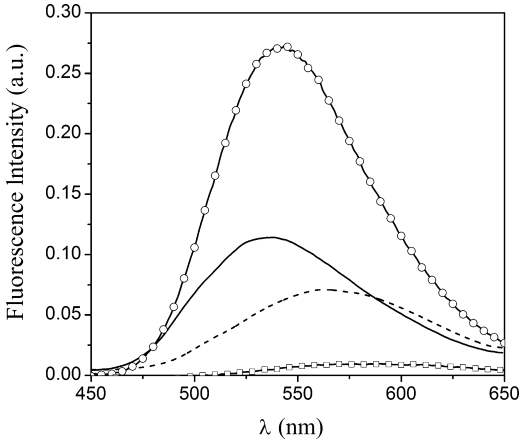


Fig. 2. Spectroscopic Behaviour of AHTC in Different Media

Fluorescence emission spectra of 25 μM AHTC in buffer (– – –) and in butanol (——) and of 1.2 μM AHTC in buffer (–□–□–) and in the presence of BSA at $[AHTC]_{tot}/[BSA]_{tot}=0.5$ (—○—). AHTC was excited at 430 nm.

(ΔH_b), determined by ITC, was kept constant. Individual thermograms measured at $[AHTC]_{tot}/[BSA]_{tot} \geq 10$ were fit and output K_b^{app} values were averaged. The robustness of the fits was assessed from the agreement of the K_b^{app} values obtained by fitting the DSC curves considering the entire range of the heat absorption peak or only the 12.5, 25 and 50% of the endotherms where potential irreversible states were expected to be less populated.

RESULTS AND DISCUSSION

Fluorescence Changes Upon AHTC–BSA Interaction Fluorometric studies of several TC derivatives indicate that these compounds share the polarity sensitivity of classical solvatochromic probes, such as arylaminonaphthalene sulfonates (ANS).[29,30] The fluorescence intensity is enhanced in non-polar environments as a consequence of an increase in the quantum yield, which is accompanied by a spectral shift towards lower wavelengths.[29,30]

We found similar polarity sensitivity for AHTC fluorescence. In comparison with the emission in buffer, the spectrum of AHTC in butanol was blue-shifted by 30 nm and the intensity increased about twofold (Fig. 2). This enhancement suggested an increase in the quantum yield since the absorbance of AHTC was the same in these two solvents (data not shown). Similarly, a marked increase in the fluorescence intensity of the drug along with a hypsochromic shift of 26 nm was observed in the presence of BSA (Fig. 2). The correspondence between the fluorescence signatures of AHTC found in media of different polarity and upon binding to BSA (Fig. 2) suggests that the bound drug is located in a low-polar environment.

Numerous binding studies indicate that the major regions of ligand binding sites in albumin are located in hydrophobic and positively charged cavities in subdomains IIA and IIIA.[20] Site I is located at subdomain IIA and has been characterized as a big and flexible pocket with positive charges in the entrance and hydrophobic chain residues inside. Site I is capable of the binding of negatively charged heterocyclic ligands as bulky as bilirubin.[20] Site II, located in subdomain IIIA, has similar physicochemical characteristics as Site I but

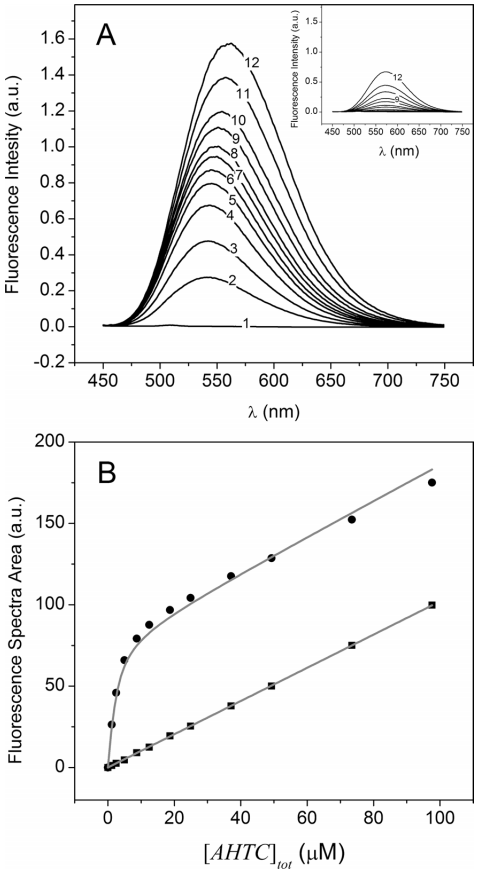


Fig. 3. Analysis of AHTC–BSA Interaction by Fluorescence Spectroscopy

(A) Fluorescence emission spectra of solutions of BSA alone (1) and at increasing concentrations of AHTC; $[AHTC]_{tot}/[BSA]_{tot}$: 0.5 (2), 1 (3), 2 (4), 3.5 (5), 5 (6), 7.5 (7), 10 (8), 15 (9), 20 (10), 30 (11) and 40 (12). Inset: Fluorescence emission spectra of solutions at the same concentrations of AHTC in buffer alone. The initial protein concentration was 2.5 μM. Spectra were corrected for inner filter effects. (B) Titration curve of BSA with AHTC. The data correspond to the area under the curves of the spectra shown in (A), in the absence (■) or the presence of BSA (●). The lines represent the fits obtained using Eq. 1.

the pocket is smaller and less flexible. Therefore, Site II usually binds smaller ligands, such as diazepam.[20] Displacement experiments employing warfarin and bilirubin (Site I) and diazepam (Site II) suggested that TC derivatives bind to the Site I at subdomain IIA of BSA.[31] On the basis of our fluorescence results, we postulate that AHTC would bind to a buried binding site excluded from water in subdomain IIA. This tentative binding location correlates with the big, planar and aromatic structure of AHTC[13,14] and the predominant anionic form of the drug.

Binding Properties Assessed by Fluorescence Spectroscopy We took advantage of the distinctive fluorescence signatures of AHTC upon interacting with BSA in order to estimate the binding parameters. Figure 3A shows the fluorometric titration of BSA with AHTC, along with the blank experiments (Fig. 3A, inset). The progressive increase in fluorescence intensity and the spectral red-shift (Fig. 3A) indicate the saturation of the protein binding sites. Figure 3B shows the integrated fluorescence signals for AHTC in the presence and absence of BSA as a function of the drug concentration after correcting for dilution. The fit of the fluorescence data according to Eq. 1 suggests that BSA would bind one molecule of AHTC with a K_b^{app} of $7\times10^5\ M^{-1}$ (Table 1). This value lies within the range of association constants re-

Table 1. Thermodynamic Binding Parameters for AHTC–BSA Interaction at 25 °C[a)]

	n	$K_b^{app} \times 10^{-5}/M^{-1}$	ΔH_b/kcal mol^{-1}	$T\Delta S_b$/kcal mol^{-1}
Fluorescence	0.97±0.02	6.6±0.6		
ITC[b)]	1.27±0.04	2.2±0.3	−6.1±0.3	1.2
DSC	1.6±0.1[c)]	2±[d)]		

a) The standard error only considers the fitting dispersion. *b*) Mean values of three independent experiments. *c*) Value obtained from Fig. 6. *d*) Average value estimated according to the formalism described in ref. 28 with $n=1$ and $\Delta H_b = -6.1$ kcal mol^{-1} as determined by ITC measurements.

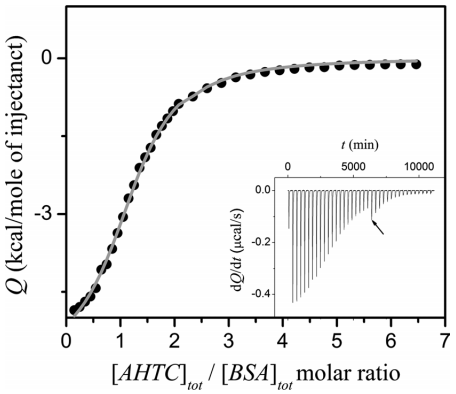


Fig. 4. Calorimetric Titration of BSA with AHTC

Representative binding isotherm and the best fit curve according to a model of single set of binding sites. Inset: Heat flux profile associated with the injections of ligand in the calorimetric cell. The arrow indicates the shot where the volume of titrant was increased.

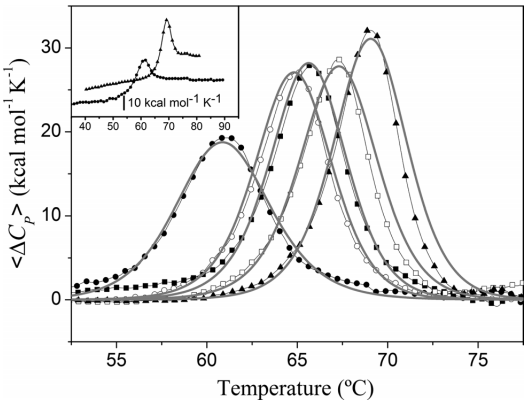


Fig. 5. Changes in BSA Thermostability Upon AHTC Binding

Experimental DSC profiles for the unfolding of BSA alone (●) and in the presence of increasing drug concentration at $[AHTC]_{tot}/[BSA]_{tot}$: 10 (○), 15 (■), 30 (□), and 65 (▲). Inset: Representative traces before baseline subtraction.

Table 2. Thermal Unfolding Parameters of BSA at Different Ligand/Protein Molar Ratios

$[AHTC]_{tot}/[BSA]_{tot}$	T_m/°C	ΔH_m/kcal mol^{-1}	ΔH_{vH}/kcal mol^{-1}
0	60.9	129	129
1	61.8	90	162
5	63.7	102	159
10	64.8	144	167
15	65.6	155	159
20	66.4	132	196
30	67.1	145	176
40	68.2	171	179
65	68.9	150	196

ported for negatively charged drugs.[19)]

Thermodynamic Binding Parameters Obtained by ITC ITC experiments were carried out in order to get thermodynamic binding parameters. Figure 4 shows a representative calorimetric titration experiment. The exothermic heat peaks exhibited a monotonic decrease with the addition of drug until saturation was reached (Fig. 4A). The dependence of heat evolved upon BSA–AHTC interaction was characteristic for a single set of binding sites (Fig. 4B). The affinity and stoichiometry for AHTC binding determined by ITC agreed quite well with those values estimated by fluorescence (Table 1).

The binding reaction had a favorable enthalpy, ΔH_b of about -6 kcal mol^{-1} (Table 1). This global parameter involves numerous contributions such as bulk hydration effects, direct non-covalent interactions at the protein–ligand interface and conformational changes of the interacting partners.[32,33)] By way of comparison, ΔH_b ranging from 2 to 3 kcal mol^{-1} have been reported for various TC derivatives interacting with BSA.[29)] We obtained a somewhat different value for AHTC, but the methods of determination and the experimental conditions may not be directly comparable.

The $\Delta H_b < 0$ was accompanied by a favorable entropy contribution ($T\Delta S_b > 0$) as determined by the titration experiments (Table 1). On binding, an entropic penalty accounting for the reduction in the number of particles and their translational and conformational degrees of freedom in the complex are expected.[32,33)] In this sense, we have reported that aniline naphthalene sulfonate (ANS) derivatives induce an overall tightening of the BSA structure which may contribute to an unfavorable conformational entropy change.[24,34)] The positive entropy contribution observed for AHTC–BSA interaction suggests the release of structural water molecules involved in a network of interactions.[32,33)]

DSC Analysis Protein stability is modulated by ligands that bind with a moderate or high affinity as a thermodynamic consequence of the coupling of the unfolding and binding equilibria. This effect is accounted for by a shift of T_m along with a change in ΔH_m, being more marked for high affinity protein–ligand interactions.[24,26,35,36)] We employed DSC as an analytical tool to estimate the binding parameters.

Figure 5 shows representative experimental endotherms obtained for BSA alone and at increasing $[AHTC]_{tot}/[BSA]_{tot}$ before (inset) and after baseline subtraction. The thermal stability of an AHTC solution was confirmed by the invariability of the absorbance spectra throughout the temperature range of the DSC scans (data not shown). The thermally induced unfolding of free BSA was characterized by a denaturation temperature (T_m°) of 60.9 °C, an unfolding enthalpy (ΔH_m°) of 129 kcal mol^{-1} and a heat capacity change (ΔC_p°) of 5.9 kcal mol^{-1} K^{-1}, respectively (Fig. 5, Table 2). The protein unfolding parameters were in excellent agreement with those reported previously.[24)] The cooperative unit was near 1 (Table 2) suggesting a two-state unfolding process[22)] (see DSC measurements section in Materials and Methods).

AHTC binding increased BSA thermal stability, as indicated by the shift of the thermograms to higher temperatures when the drug concentration was increased (Fig. 5). Compared with the free protein, an increase of 8 °C and

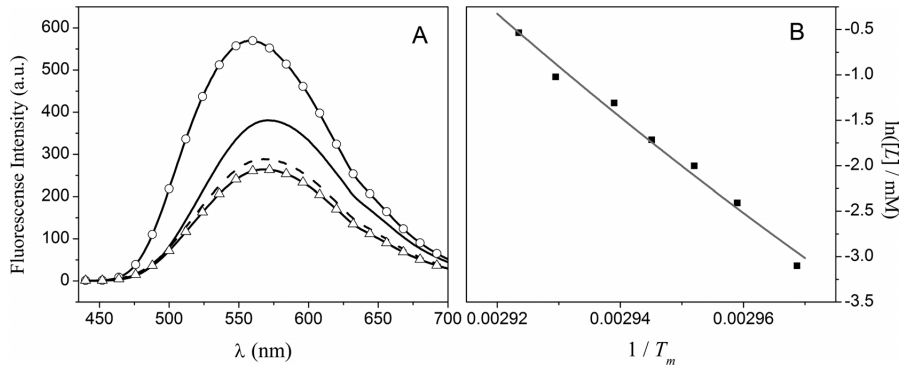


Fig. 6. Analysis of Binding Stoichiometry for the AHTC–BSA Complex from DSC Data

(A) Preferential binding of AHTC to native BSA. Fluorescence emission spectra of AHTC in buffer alone at 25 °C (——), and 75 °C (– – –), and in the presence of BSA at 25 °C (—○—) and 75 °C (—△—).$[P]_{tot}$=2.5 μM, $[L]_{tot}$=162.5 μM. (B) Plot of ln($[AHTC]_{tot}$/mM) *versus* $1/T_m$ at $[AHTC]_{tot}/[BSA]_{tot}\geq 5$. The data were analyzed according to Eq. 2 and the line is the best fit obtained with A=2762.6±0.7 and n=1.6±0.1.

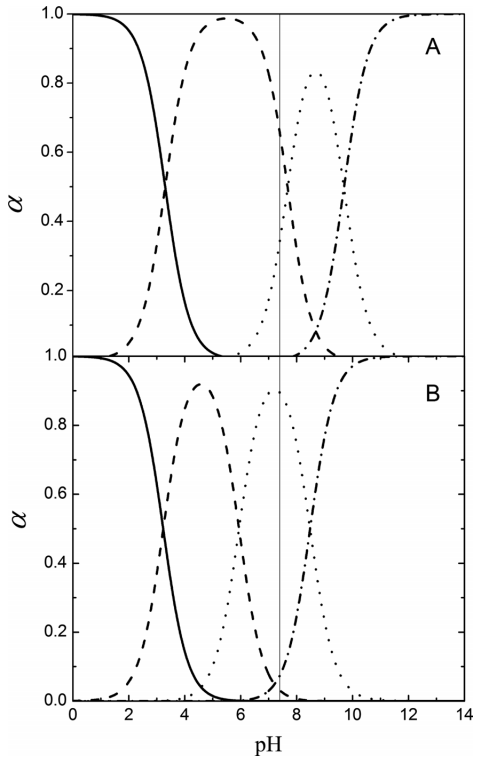


Fig. 7. Effect of pH on the Species Distribution Profile of TC (A) and AHTC (B)

Protonated species (——), neutral species (– – –), monovalent anionic species (···) and divalent anionic species (–·–). The vertical line indicates the experimental pH employed in this study (pH 7.4). The acidic constant values are: TC[43] pK_1=3.30, pK_2=7.68, pK_3=9.69 and AHTC[44] pK_1=3.23, pK_2=5.94, pK_3=8.48.

21 kcal mol^{-1} in T_m and ΔH_m, respectively, was seen at $[AHTC]_{tot}/[BSA]_{tot}$=65 (Fig. 5, Table 2). The calorimetric trend indicates that native BSA preferentially binds AHTC with a moderate affinity.

For protein unfolding processes that involve ligand dissociation from the native protein, T_m keeps increasing with $[L]_{tot}$ even at molar ratios for which binding sites are essentially fully occupied.[35,36] This dependence allows the estimation of n if model-based expressions for the binding polynomial are supplied.[36] At constant $[P]_{tot}$ and $[L]_{tot} \gg [P]_{tot}$, the equation that entails T_m and $[L]_{tot}$ is[24,36]:

$$\ln([L]_{tot}/M) = \frac{A}{n} + \left(\frac{\Delta C_p^\circ T_m - \Delta H_m^\circ - n\Delta H_b}{nR}\right)\frac{1}{T_m} + \frac{\Delta C_p^\circ \ln(T_m/T_m^\circ)}{nR} \quad (2)$$

where R is the gas constant, A is a constant, and the other parameters are as defined previously. We have successfully used this approach to estimate the number of binding sites for different dyes on serum albumins.[24,28]

In order to confirm the preferential binding of AHTC to native BSA, as suggested by our calorimetric results (Fig. 5, Table 2), the emission spectra of free and bound AHTC at different temperatures were compared. At $[AHTC]_{tot}/[BSA]_{tot}$=65, the fluorescence features of AHTC at $T \gg T_m$, *i.e.*, in the presence of the denatured protein, were essentially the same as those found in buffer (Fig. 6A) indicating that binding to the unfolded state, if any, can be neglected.

In view of this, n was estimated from the plot of ln($[AHTC]_{tot}$/mM) *versus* T_m^{-1} (Fig. 6B) according to Eq. 2. The values of ΔC_p°, ΔH_m° and T_m° were obtained from the experimental thermogram of free BSA, whereas the ΔH_b was obtained from ITC measurements. These parameters were held constant during the nonlinear curve fit of the data in Fig. 6B. The best fit yielded a value of n=1.6±0.1 (Table 1). To minimize the number of parameters, the data were also fit with a similar equation but assuming a temperature-independent K_b^{app}, *i.e.*, neglecting the ΔH_b term in Eq. 2. In this case, we obtained a value of n=1.5±0.1. Despite the approximations inherent in this method, the DSC analysis suggests that between one and two molecules of AHTC bind to native BSA, in good agreement with previous determinations (Table 1).

In addition, K_b^{app} was assessed from the DSC experiments as described in Experimental. Individual endotherms acquired at $[AHTC]_{tot}/[BSA]_{tot}\geq 10$ were fit assuming one binding site on the native protein. Figure 5 shows a comparison between the experimental and fit curves. The discrepancies at $T > T_m$ probably arise from some aggregation process which was not taken into account in the theoretical model. Additional fits using up to the 50% of the data of the experimental unfolding traces yielded similar K_b^{app} values. With this procedure, we estimated an average affinity constant of about 2×10^5 M^{-1}, in satisfactory agreement with that directly determined by ITC (Table 1).

Species Distribution Profile Analysis The apparent binding constant of the AHTC–BSA complex was approxi-

mately one order of magnitude higher than those reported for TC and other TC derivatives.[37—39] Although there may be a correlation between the higher hydrophobicity of AHTC relative to other TC derivatives[16,17] and the higher affinity, further contributions such as electrostatic forces should be considered.[40—42] Indeed, the relevance of electrostatic interaction in TC binding to BSA has been discussed previously.[31] Thus, the species distribution profile as a function of pH (Fig. 7) revealed a notable difference between AHTC and its parent compound. At physiological pH, AHTC is mainly found as a monovalent anion and only a 3% ($\alpha_{AHTC}=0.03$) is present in the neutral form (Fig. 7B). Having in mind that $K_b^{app}=\alpha K_b$, K_b being the intrinsic thermodynamic binding constant, the distribution profile indicates that under our experimental condition BSA would bind a negatively charged AHTC molecule with a K_b *ca.* $10^5\ M^{-1}$ or a neutral form with a much higher affinity such that the K_b^{app} *ca.* $10^5\ M^{-1}$. In addition, the ratios between the total anionic and neutral species for the two drugs are quite different at physiological pH (Fig. 7): *ca.* 30 and 0.5 for AHTC and TC, respectively. Therefore, ionic interactions may be involved in the distinct binding of these drugs to serum albumins.

CONCLUSION

In this work we have characterized the interaction of the highly toxic TC derivative, AHTC, with BSA. By using three complementary analytical techniques, we showed that one molecule of AHTC interacts with BSA with a moderate affinity, in a binding event favored by enthalpic and entropic contributions. Drug binding probably involves both hydrophobic and electrostatic interactions. The fact that the affinity of AHTC for albumin is higher than that exhibited by other TC derivatives may have an impact on the biodisponibility of pharmacological drugs and the dynamic distribution of the toxic derivative due to mechanisms of competition for the binding site. This is particularly interesting due to the extensive use of TC derivatives in medicine and the increasing number of applications differing from their classical antimicrobial actions.

Acknowledgements L.I.R., G.D.F. and S.A.D. are members of Consejo Nacional de Investigaciones Científicas y Tecnológicas (CONICET). M.I.B. and R.A.F. thank CONICET for the fellowships granted. This work was supported by grants from CONICET, Secretaría de Ciencia y Tecnología (SECyT-UNC) and Foncyt. The authors thank Dr. Lucia Bianconi (UFRJ, Brazil) for ITC facilities. Language assistance by C. Mosconi is gratefully acknowledged.

REFERENCES

1) Chopra I., Roberts M., *Microbiol. Mol. Biol. Rev.*, **65**, 232—260 (2001).
2) Tagliavini F., Forloni G., Colombo L., Rossi G., Girola L., Canciani B., Angeretti N., Giampaolo L., Peressini E., Awan T., De Gioia L., Ragg E., Bugiani O., Salmona M., *J. Mol. Biol.*, **300**, 1309—1322 (2000).
3) Forloni G., Colombo L., Girola L., Tagliavini F., Salmona M., *FEBS Lett.*, **487**, 404—407 (2001).
4) Cardoso I., Merlini G., Saraiva M. J., *FASEB J.*, **17**, 803—809 (2003).
5) Dürckheimer W., *Angew. Chem. Int. Ed. Engl.*, **14**, 721—734 (1975).
6) Hasan T., Kochevar I. E., McAuliffe D. J., Cooperman B. S., Abdulah D., *J. Invest. Dermatol.*, **83**, 179—183 (1984).
7) Milne M. D., *Annu. Rev. Pharmacol.*, **10**, 119—136 (1965).
8) Halling-Sørensen B., Sengeløv G., Tjørnelund J., *Arch. Environ. Contam. Toxicol.*, **42**, 263—271 (2002).
9) Beliakova M. M., Bessonov S. I., Sergeyev B. M., Smirnova I. G., Dobrov E. N., Kopylov A. M., *Biochemistry* (Mosc.), **68**, 182—187 (2003).
10) Hasan T., Allen M., Cooperman B. S., *J. Org. Chem.*, **50**, 1755—1757 (1985).
11) Kühne M., Hamscher G., Körner U., Sched D., Wenzel S., *Food Chem.*, **75**, 423—426 (2001).
12) Stoel L. J., Newman E. C., Asleson G. L., Frank C. W., *J. Pharm. Sci.*, **65**, 1794—1799 (1976).
13) Palenik G. J., Mathew M., Restivo R., *J. Am. Chem. Soc.*, **100**, 4458—4464 (1978).
14) Stezowski J. J., *J. Am. Chem. Soc.*, **98**, 6012—6018 (1976).
15) Goodman J. J., Matrishin M., Backus E. J., *J. Bacteriol.*, **69**, 70—72 (1955).
16) Fernández R. A., Dassie S. A., *J. Electroanal. Chem.*, **585**, 240—249 (2005).
17) Fernández R. A., Dassie S. A., *J. Electroanal. Chem.*, **624**, 121—128 (2008).
18) Craig W. A., Kunin C. M., *Annu. Rev. Med.*, **27**, 287—300 (1976).
19) Kragh-Hansen U., *Pharmacol. Rev.*, **33**, 17—53 (1981).
20) Kragh-Hansen U., Chuang V. T., Otagiri M., *Biol. Pharm. Bull.*, **25**, 695—704 (2002).
21) Rosso S. B., Gonzalez M., Bagatolli L. A., Duffard R. O., Fidelio G. D., *Life Sci.*, **63**, 2343—2351 (1998).
22) Privalov P. L., *Adv. Protein Chem.*, **33**, 167—241 (1979).
23) Sanchez-Ruiz J. M., *Biophys. J.*, **61**, 921—935 (1992).
24) Celej M. S., Dassie S. A., Freire E., Bianconi M. L., Fidelio G. D., *Biochim. Biophys. Acta*, **1750**, 122—133 (2005).
25) Brandts J. F., Lin L. N., *Biochemistry*, **29**, 6927—6940 (1990).
26) Shrake A., Ross P. D., *Biopolymers*, **32**, 925—940 (1992).
27) Straume M., Freire E., *Anal. Biochem.*, **203**, 259—268 (1992).
28) Celej M. S., Dassie S. A., González M., Bianconi M. L., Fidelio G. D., *Anal. Biochem.*, **350**, 277—284 (2006).
29) Popov P. G., Vaptzarova K. I., Kossekova G. P., Nikolov T. K., *Biochem. Pharmacol.*, **21**, 2363—2372 (1972).
30) Takahashi M., Altschmied L., Hillen W., *J. Mol. Biol.*, **187**, 341—348 (1986).
31) Khan M. A., Muzammil S., Musarrat J., *Int. J. Biol. Macromol.*, **30**, 243—249 (2002).
32) Jelesarov I., Bosshard H. R., *J. Mol. Recognit.*, **12**, 3—18 (1999).
33) Tame J. R. H., O'Brien R., Ladbury J. E., "Isothermal Titration Calorimetry of Biomolecules," Vol. 2, ed. by Ladbury J. E., Chowdrhy B. Z., John Wiley & Sons, Chichester, 1998, pp. 27—38.
34) Celej M. S., Montich G. G., Fidelio G. D., *Protein Sci.*, **12**, 1496—1506 (2003).
35) Cooper A., Nutley M. A., Wadood A., "Differential Scanning Microcalorimetry," Vol. 11, ed. by Harding S. E., Chowdrhy B. Z., Oxford University Press, New York, 2000, pp. 287—318.
36) Fukada H., Sturtevant J. M., Quiocho F. A., *J. Biol. Chem.*, **258**, 13193—13198 (1983).
37) Powis G., *J. Pharm. Pharmacol.*, **26**, 113—118 (1974).
38) Vallner J. J., *J. Pharm. Sci.*, **66**, 447—465 (1977).
39) Zia H., Price J. C., *J. Pharm. Sci.*, **65**, 226—230 (1976).
40) Peters T. J., "All About Albumin: Biochemistry, Genetics, and Medical Applications," 1st ed., Elsevier, San Diego, 1995.
41) Böhm H.-J., "Prediction of Non-bonded Interactions in Drug Design," Vol. 1, ed. by Böhm H.-J., Schneider G., Wiley-VCH Verlag GmbH & Co., Weinheim, 2003, pp. 3—20.
42) Williams M. A., Ladbury J. E., "Hydrogen Bonds in Protein–Ligand Complexes," Vol. 6, ed. by Böhm H.-J., Schneider G., Wiley-VCH Verlag GmbH & Co., Weinheim, 2003, pp. 137—161.
43) Stephens C. R., Murai K., Brunings K. J., Woodward R. B., *J. Am. Chem. Soc.*, **78**, 4155—4158 (1956).
44) de Siqueira J. M., Carvalho S., Paniago E. B., Tosi L., Beraldo H., *J. Pharm. Sci.*, **83**, 291—295 (1994).